The Eurasia Proceedings of Science, Technology, Engineering & Mathematics (EPSTEM)
ISSN: 2602-3199

The Eurasia Proceedings of Science, Technology, Engineering & Mathematics (EPSTEM), 2023

Volume 24, Pages 243-256

IConTech 2023: International Conference on Technology

A Numerical Study of the Efficiency of the Sono Galvano-Fenton Process as a Tertiary Treatment Technique for the Wastewater Reuse in Agriculture

Kaouther Kerboua
National Higher School of Technology and Engineering

Abstract: In the present study, the Sono-Galvano-Fenton process is studied numerically as a tertiary treatment process for treated wastewater reuse in irrigation, with in situ generation of the Fenton's reagent and catalyst, i.e., H_2O_2 and Fe^{2+}. The sonochemical pathway is examined as a source of hydrogen peroxide under the pre-optimized condition of acoustic frequency, 200 kHz. The macroscopic model accounting for the performance of the single acoustic cavitation bubble and the bubble population density is combined with the Fe/Cu galvanic cell operating in acidic conditions (pH 3), following a cumulative and instantaneous production approach in terms of Fenton's reagent. The combination is optimized based on the rate of hydroxyl radicals generated by the Galvano-Fenton process, as a non-selective powerful oxidant against recalcitrant pollutants, then considering the synergetic effect of the hybrid process in terms of $HO^{\bullet}$ pumped sonochemically and via the Fenton based pathway, treated using simulations of the isolated processes then their combined configuration following both aforementioned approaches.

Keywords: Numerical model, Synergy, Hydroxyl radical, Ultrasounds, Galvano Fenton, Simulation.

Introduction

Ultrasounds as a carrier of mechanical power is used in chemistry in the so-called sonochemical processes (Mason, 1999). Sonochemistry is defined as the chemistry induced by ultrasounds indirectly, through the microscopic process of acoustic cavitation bubble (Leighton, 1994). Acoustic cavitation bubble is formed by heterogeneous nucleation as small pockets of gas are present in the sonicated liquid, it then oscillates under the pace of the ultrasonic wave, it accumulates energy so that a chemical mechanism is activated starting with the decomposition of water molecules. Under oxygen atmosphere, the hydrogen, hydroxyl and oxygen radicals that appear in the liquid medium interact to form new molecules, including hydrogen peroxide (Dalodiere et al., 2016; Ziembowicz et al., 2017). Hydrogen peroxide is a powerful oxidant used as a precursor fro hydroxyl radicals (He et al., 1988) in advanced oxidation processes (Palit, 2012). It is also the well-known reagent of the Fenton reaction (Barbusinski, 2009). The combination of ultrasounds with Fenton based processes may be an efficient option for the in-situ production of hydrogen peroxide, especially if the integration considers a method for the in-situ production of the Fenton's catalyst, namely ferrous ions. In the present paper, direct continuous sonication is integrated to the Galvano-Fenton process studied in our previous papers (Kerboua, 2022; Kerboua et al., 2021) in order to investigate numerically the possibility of producing autonomously hydrogen peroxide. The proposed model considers the microscopic and macroscopic effect of sonication in terms of the sonochemical production of H_2O_2, and the simultaneous performance of the Sono-Galvano-Fenton process. A preliminary study for the optimization of acoustic frequency condition is carried out using modeling and simulation.

Method

Configuration of the Modelled Process

The integrated process accounts for direct continuous sonication using a transducer placed at the bottom of the reactor, and delivering an acoustic amplitude of1.5 atm. The studied frequencies are supposed to vary from 20 to 800 kHz, including 200, 300, 360, 443, 500 and 600 kHz. The adopted acoustic frequency is selected based on the optimal reactor scale production of hydrogen peroxide.

The Galvano-Fenton process is designed by immersing a galvanic cell of iron anode (sacrificial anode) and copper cathode within an acidified electrolyte, at the pH condition allowing the formation of ferrous ions according to the Pourbaix diagram, i.e., pH 3. Hydrogen peroxide is produced sonochemically while the spontaneous corrosion of iron occurs, inducing the Fenton reaction. The process is simulated considering a corrosion current of 300 µA, determined experimentally during the preliminary test described in our previous works (Kerboua, 2022). The Galvano-Fenton system is modeled by combining electrochemical reactions taking place at the anode and the cathode with chemical reactions related to the Fenton mechanism occurring in the bulk liquid volume. The Fenton based mechanism has been validated experimentally in our previous studies using blank tests (Gasmi et al. 2020; Gasmi et al., 2020). The specifications of the parameters corresponding to the aformentionned described configuration are all reported in Table. 1. A schema of the integrated process is presented in Fig.1.

Table 1. Specifications of the Sono-Galvano-Fenton cell

Parameter	S1pecification
Type of sonication	Direct
Mode of sonication	Continuous
Acoustic frequency to be tested	20, 200, 360, 443, 600, 800 kHz
Acoustic amplitude	1.5 atm
Electrodes form	rectangular smooth plates
Immersed electrodes surface	12 cm^2
Electrolyte volume	100 mL
Electrodes disposition	In parallel
Electrolyte nature	Acidified water (H_2SO_4)
pH	3
Electrical connection	External wire
Ionic displacement	Aided by a magnetic stirring
Initial concentration of hydrogen peroxide	0 mM

Numerical Modelling

The Microscopic Effect Of Sonication

The single bubble dynamics is governed by the modified Keller-Miksis equation accounting for the non-equilibrium of evaporation and condensation of water molecules at the gas-liquid interface (Kerboua & Hamdaoui, 2019; Yasui, 1997), as expressed in Eq. 1. The present numerical model is based on combining both sonochemical activity of single acoustic cavitation bubble and kinetic evolution of number density of bubbles within a control volume of a sonochemical reactor filed of water saturated with oxygen.

$$\ddot{R}-\frac{\left(c+\dot{R}\right)}{\rho_L\left(cR-\dot{R}R+\frac{\dot{m}R}{\rho_L}\right)+4\mu}\left(P_g-\frac{26}{R}-4\mu\frac{\dot{R}}{R}-\ P_\infty+P_a sin\left(2\pi f\left(t+\frac{R}{c}\right)-\bar{k}x\right)\right)$$
$$=\frac{R}{\rho_L\left(cR-\dot{R}R+\frac{\dot{m}R}{\rho}\right)+4\mu}\left(\frac{dP_g}{dt}+\frac{26\dot{R}}{R^2}+4\mu\frac{\dot{R}^2}{R^2}\right)-\frac{\rho_L(\left(3c-\dot{R}\right)+\frac{2\dot{m}}{\rho_L})\dot{R}^2}{2\left(\rho_L\left(cR-R\dot{R}+\frac{\dot{m}R}{\rho_L}\right)+4\mu\right)} \quad (1)$$
$$+\frac{\dot{m}\left(cR-R\dot{R}+\frac{\dot{m}R}{\rho_L}\right)}{\rho_L\left(cR-R\dot{R}+\frac{\dot{m}R}{\rho_L}\right)+4\mu}+\frac{\dot{m}\left(c\dot{R}+\frac{\dot{m}}{2\rho_L}\left(c+\dot{R}\right)\right)}{\rho_L\left(cR-R\dot{R}+\frac{\dot{m}R}{\rho_L}\right)+4\mu}$$

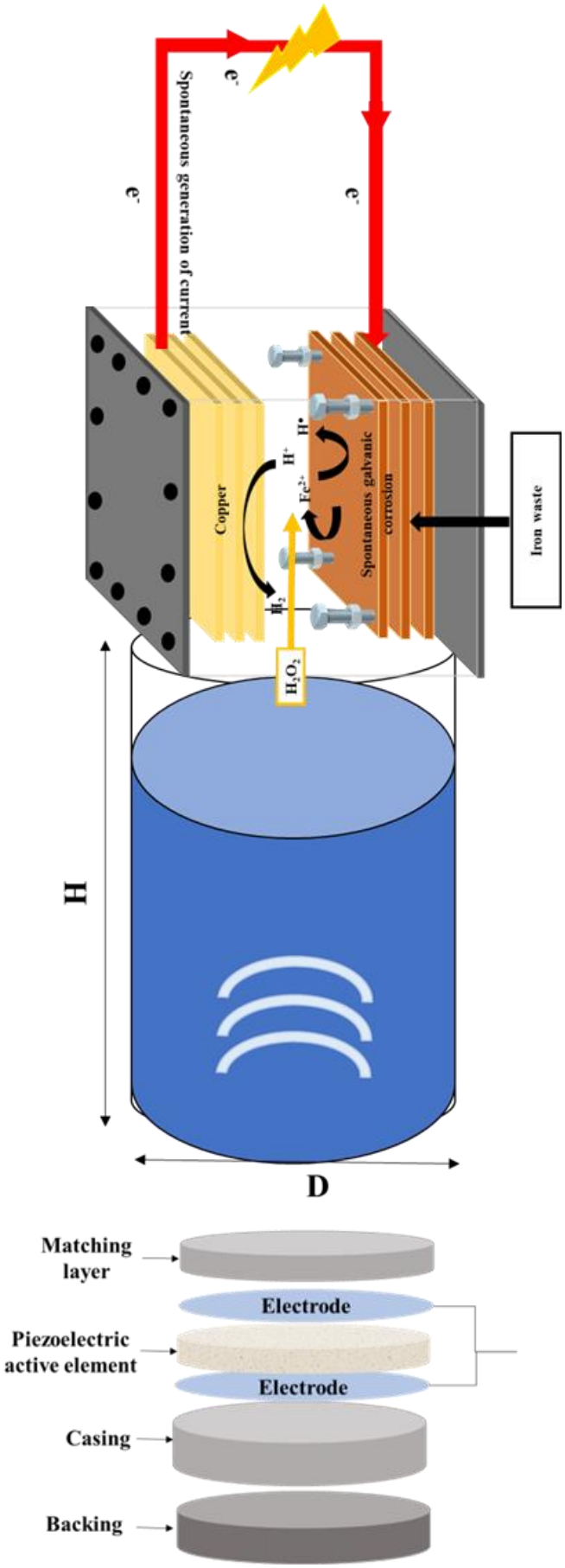

Figure 1. Schema of the integrated Sono-Galvano-Fenton process

The active bubble population is supposed to be composed of bubbles having similar equilibrium radius R_0. The value of R_0 is frequency dependent, ambient radii were selected in respect to the theoretical intervals defined by Yasui (2002) and reported by Brotchie et al. (2009). These values are limited by Blake (Atchley, 1989) and Minnaert et al. (1933) thresholds under the frequencies i.e. 20, 200, 300, 360, 443, 500, 600 and 800 kHz. The assumed acoustic amplitude is equivalent to an acoustic intensity 0.77 W/cm^2 according to Eq. 2 (Authier et al., 2018), and a power density is also expressed according to Eq. 3.

$$P_a = \sqrt{2\rho_L c I} \tag{2}$$

$$P = \frac{{P_a}^2 A}{2\rho_L c V_R} \tag{3}$$

Each single bubble constitutes a microreactor of spherical form and varying volume, the volume variation is then expressed by Eq. 4.

$$\frac{dV}{dt} = 4\pi R^2 \frac{dR}{dt} \tag{4}$$

While the volume of each microreactor varies in function of time, temperature and pressure within it evolves according to Eq. 5 and 6, respectively

$$-P_g 4\pi R^2 \dot{R} - \frac{1}{3}\sum_{j=1}^{45} \Delta H_j r_j 4\pi R^3 + 4\pi R^2 \frac{m}{M_{H_2O}} C_{V_{H2O}} T = \frac{\lambda}{\xi} 4\pi R^2 (T - T_\infty) + \sum_{k=1}^{9} n_k C_V \dot{T} \tag{5}$$

$$\left(P_g + \frac{n^2 a}{V^2}\right)(V - nb) = nR_g T \tag{6}$$

Eq. 5 represents the heat balance applied to the single bubble volume. This heat balance considers the single acoustic cavitation bubble as opened to heat exchange through thermal diffusion across the thin heat transfer layer at the bubble interface, and evaporation and condensation processes carrying water molecules enthalpy toward and outward the bubble volume as illustrated in Fig. 1. Each microreactor is also considered open to mass transfer through physical phenomenon of simultaneous evaporation and condensation of water molecules at bubble interface as shown in Fig. 1, whose kinetics is governed by Hertz-Knudsen equation shown in Eq. 7 (Yasui, 1996).

$$\dot{m} = M_{H_2O} \frac{dn_{H_2O}}{dt} = \frac{\sqrt{M_{H_2O}}}{\sqrt{2\pi R_g}} \alpha \frac{1}{\sqrt{T}} (P_v - P_i) \tag{7}$$

The oscillation of active acoustic cavitation bubbles is particularly characterized by spectacular elevations of pressures and temperatures attaining 1000 bar and 6000 K, respectively, under 1.5 atm of acoustic amplitude (Kerboua & Hamdaoui, 2017, 2018) and occurring when the bubble contracts to its minimal size and collapses. The harsh conditions then attained activate a considerable number of elementary reactions initiated by the thermal decomposition of H_2O into hydroxyl and hydrogen radicals, and the reaction of H_2O and O_2 as shown below.

$H_2O \rightarrow H^\bullet + {}^\bullet OH$

$O_2 + H_2O \rightarrow {}^\bullet OH + HO_2^\bullet$

In the present model, 45 elementary reactions are expected to occur according to the schema reported in Table 2 and initially suggested by Yasui (1997) and inspired from Baulch et al. (1972, 1974, 1976) and Kamath et al. (1993). The molar rate related to ith reaction is expressed in Eq. 8. Hence, the molar rate due to chemical reactions and related to the kth species among the nine involved in the model is represented by Eq. 9.

$$r_i = A_i e^{\left(\frac{-E_i}{R_g T}\right)} \prod_{k=1}^{9} (c_k)^{\vartheta_{ki}} \qquad i = \overline{1,45} \tag{8}$$

$$\frac{dn_k}{dt} = \frac{4}{3}\pi R^3 \sum_{i=1}^{45} (\vartheta'_{ki} - \vartheta_{ki})\, A_i e^{\left(\frac{-E_i}{RT}\right)} \prod_{k=1}^{9} (c_k)^{\vartheta_{ki}} \qquad k = \overline{1,9} \tag{9}$$

According to Eqs. 7, 8 and 9, the molar yields of the $HO^{\bullet}$ and H_2O_2 involved in the chemical schema can be expressed in terms of molar concentration as shown in Eqs. 10 and 11.

$$\frac{dc_{HO^{\bullet}}}{dt} = \sum_{i=1}^{45} (\vartheta'_{HO^{\bullet}\,i} - \vartheta_{HO^{\bullet}\,i})\, A_i e^{\left(\frac{-E_i}{R_g T}\right)} \prod_{k=1}^{9} (c_k)^{\vartheta_{ki}} - 3c_{HO^{\bullet}} \frac{\dot{R}}{R} \tag{10}$$

$$\frac{dc_{H_2O_2}}{dt} = \sum_{i=1}^{45} (\vartheta'_{H_2O_2\,i} - \vartheta_{H_2O_2\,i})\, A_i e^{\left(\frac{-E_i}{R_g T}\right)} \prod_{k=1}^{9} (c_k)^{\vartheta_{ki}} - 3c_{H_2O_2} \frac{\dot{R}}{R} \tag{11}$$

At the macroscopic scale, the sonochemical activity of bubble population is observed within a cylindrical control volume. The energy balance applied to the control volume leads to Eq. 12, already demonstrated in a previous work of our research group (Kerboua & Hamdaoui, 2019).

$$\begin{aligned} -\sum_{j=1}^{45} \frac{4}{3}\pi \Delta H_i r_i R^3 N - \frac{4}{3}\pi\,(P_g - P_\infty - P)\big(3\dot{R}R^2N + R^3\dot{N}\big) - \sigma 4\pi(2\dot{R}RN + R^2\dot{N}) \\ - 2\pi\,\rho_L\,(3R^2\dot{R}^3N + 2R^3\dot{R}\ddot{R}N + R^3\dot{R}^2\dot{N} \\ - \left(N\sum_{i=1}^{9}\dot{n}_i u_i + N\sum_{i=1}^{9} n_i \dot{u}_i + \dot{N}\sum_{i=1}^{9} n_i u_i\right) = \frac{d}{dt}\left(\frac{P^2}{2\,\rho_L\,c^2} + \frac{\rho_L\,U^2}{2}\right) \end{aligned} \tag{12}$$

In this equation, N represents the number density of bubbles at instant t. Hence, the molar rates related to the sonochemical products ($HO^{\bullet}$, $HO_2^{\bullet}$, $H^{\bullet}$, H_2O_2, O, O_3, H_2), emerging from the reactions reported in Table 2, are expressed at reactor scale according to Eq. 13.

$$\frac{dC_k}{dt} = N\frac{4}{3}\pi R^3 \sum_{i=1}^{45} (\vartheta'_{ki} - \vartheta_{ki})\, A_i e^{\left(\frac{-E_i}{R_g T}\right)} \prod_{k=1}^{K} (C_k)^{\vartheta_{ki}} + \dot{N} n_k \tag{13}$$

C_k represents the molar concentration of the k[th] species (among $HO^{\bullet}$, $HO_2^{\bullet}$, $H^{\bullet}$, H_2O_2, O, O_3, H_2) within the control volume, while ϑ_{ki}, ϑ'_{ki}, E_i/R_g and A_i are the parameters relative to the chemical kinetics, explained and explicated in Table 2.

In order to model the integrated Sono-Galvano-Fenton process, the macroscopic sonochemical production of hydrogen peroxide retrived previously will be expressed based on zero order kinetics model, considering a constant production rate as shown in Eq. 14.

$$\frac{dC_{H_2O_2}}{dt} = k_0 \tag{14}$$

Iron constitutes the sacrificial electrode, Fe oxidizes to Fe^{2+} ($E^0 = -0.44$ V vs. SHE) according to Equation 1, in Table.3. At the cathode, the most probable reaction concerns the reduction of H^+ to form H_2 ($E^0 = 0$ V vs. SHE) according to Eq.2 in Table.3, owing to the acidity of the medium. This has been proven in a previous work conducted by our research group (Intissar Gasmi, Kerboua, Haddour, Hamdaoui, et al. 2020). The kinetics related to all of the electrochemical reactions are governed by Faraday's law (Ahmad, 2006), given in Eq. 15, and describe the evolution of the C_k concentration of the species involved in the electrochemical reactions in a function of time.

$$\frac{dC_k}{dt} = \pm\frac{i_{corr}}{nFV} \quad (15)$$

n represents the valence number; it equals 2 for reaction 1 and 1 for reaction 2. *F* is Faraday's number, which equals 96,490 C/mol. i_{corr} represents the corrosion current, while *V* constitutes the volume of the electrolyte.

Table 2. Adopted scheme of the possible reactions occurring inside an O_2/H_2O collapsing bubble (Yasui, 1997). M is the third body. A is expressed in (m^3/mol.s) for two body reaction (m^6/mol^2.s) for a three-body reaction.

i	Reaction i	A_i	b_i	E_i/R_g (K)	ΔH_i (kJ/mol)
1	$H + O_2 \Rightarrow O + {}^{\bullet}OH$	1.92×10^8	0	8270	69,17
2	$O + H_2 \Rightarrow H^{\bullet} + {}^{\bullet}OH$	5.08×10^{-2}	2.67	3166	8,23
3	${}^{\bullet}OH + H_2 \Rightarrow H^{\bullet} + H_2O$	2.18×10^2	1.51	1726	−64,35
4	${}^{\bullet}OH + {}^{\bullet}OH \Rightarrow H_2O + O$	2.1×10^2	1.4	200	−72,59
5	$H_2 + M \Rightarrow H^{\bullet} + H^{\bullet} + M$; Coef. H_2: 2.5, H_2O: 16.0	4.58×10^{13}	−1.4	52500	444,47
6	$O + O + M \Rightarrow O_2 + M$; Coef. H_2: 2.5, H_2O: 16.0	6.17×10^3	−0.5	0	−505,4
7	$O + H^{\bullet} + M \Rightarrow {}^{\bullet}OH + M$; Coef. H_2O: 5.0	4.72×10^5	−1.0	0	−436,23
8	$H^{\bullet} + {}^{\bullet}OH + M \Rightarrow H_2O + M$; Coef. H_2: 2.5, H_2O: 16.0	2.25×10^{10}	−2.0	0	−508,82
9	$H^{\bullet} + O_2 + M \Rightarrow HO_2^{\bullet} + M$; Coef. H_2: 2.5, H_2O: 16.0	2.00×10^3	0	−500	−204,8
10	$H^{\bullet} + HO_2^{\bullet} \Rightarrow O_2 + H_2$	6.63×10^7	0	1070	−239,67
11	$H^{\bullet} + HO_2^{\bullet} \Rightarrow {}^{\bullet}OH + {}^{\bullet}OH$	1.69×10^8	0	440	−162,26
12	$O + HO_2^{\bullet} \Rightarrow O_2 + {}^{\bullet}OH$	1.81×10^7	0	−200	−231,85
13	${}^{\bullet}OH + HO_2^{\bullet} \Rightarrow O_2 + H_2O$	1.45×10^{10}	−1.0	0	−304,44
14	$HO_2^{\bullet} + HO_2^{\bullet} \Rightarrow O_2 + H_2O_2$	3.0×10^6	0	700	−175,35
15	$H_2O_2 + M \Rightarrow {}^{\bullet}OH + {}^{\bullet}OH + M$; Coef. H_2: 2.5, H_2O: 16.0	1.2×10^{11}	0	22900	217,89
16	$H_2O_2 + H^{\bullet} \Rightarrow H_2O + {}^{\bullet}OH$	3.2×10^8	0	4510	−290,93
17	$H_2O_2 + H^{\bullet} \Rightarrow H_2 + HO_2^{\bullet}$	4.82×10^7	0	4000	−64,32
18	$H_2O_2 + O \Rightarrow {}^{\bullet}OH + HO_2^{\bullet}$	9.55	2	2000	−56,08
19	$H_2O_2 + {}^{\bullet}OH \Rightarrow H_2O + HO_2^{\bullet}$	1.00×10^7	0	900	−128,67
20	$O_3 + M \Rightarrow O_2 + O + M$; Coef. O_2: 1.64; Coef. O_2: 1.63, H_2O: 15	2.48×10^8	0	11430	109,27
21	$O_3 + O \Rightarrow O_2 + O_2$	5.2×10^6	0	2090	−396,14
22	$O_3 + {}^{\bullet}OH \Rightarrow O_2 + HO_2^{\bullet}$	7.8×10^5	0	960	−164,92
23	$O_3 + HO_2^{\bullet} \Rightarrow O_2 + O_2 + {}^{\bullet}OH$	1×10^5	0	1410	−121,92
24	$O_3 + H^{\bullet} \Rightarrow HO_2^{\bullet} + O$	9×10^6	0.5	2010	−135,65
25	$O_3 + H^{\bullet} \Rightarrow O_2 + {}^{\bullet}OH$	1.6×10^7	0	0	−96,2
26	$O + {}^{\bullet}OH \Rightarrow H + O_2$	7.18×10^5	0.36	−342	-69,17
27	$H^{\bullet} + {}^{\bullet}OH \Rightarrow O + H_2$	2.64×10^{-2}	2.65	2245	-8,23
28	$H^{\bullet} + H_2O \Rightarrow {}^{\bullet}OH + H_2$	1.02×10^3	1.51	9370	64,35
29	$H_2O + O \Rightarrow {}^{\bullet}OH + {}^{\bullet}OH$	2.21×10^3	1.4	8368	72,59
30	$H^{\bullet} + H^{\bullet} + M \Rightarrow H_2 + M$; Coef. H_2: 2.5, H_2O: 16.0	2.45×10^8	−1.78	480	-444,47
31	$O_2 + M \Rightarrow O + O + M$; Coef. H_2: 2.5, H_2O: 16.0	1.58×10^{11}	−0.5	59472	505,4
32	${}^{\bullet}OH + M \Rightarrow O + H^{\bullet} + M$; Coef. H_2O: 5.0	4.66×10^{11}	−0.65	51200	436,23
33	$H_2O + M \Rightarrow H^{\bullet} + {}^{\bullet}OH + M$; Coef. H_2: 2.5, H_2O: 16.0	1.96×10^{16}	−1.62	59700	508,82
34	$HO_2^{\bullet} + M \Rightarrow H^{\bullet} + O_2 + M$; Coef. H_2: 2.5, H_2O: 16.0	2.46×10^9	0	24300	204,8
35	$O_2 + H_2 \Rightarrow H^{\bullet} + HO_2^{\bullet}$	2.19×10^7	0.28	28390	239,67
36	${}^{\bullet}OH + {}^{\bullet}OH \Rightarrow H^{\bullet} + HO_2^{\bullet}$	1.08×10^5	0.61	18230	162,26
37	$O_2 + {}^{\bullet}OH \Rightarrow O + HO_2^{\bullet}$	3.1×10^6	0.26	26083	231,85
38	$O_2 + H_2O \Rightarrow {}^{\bullet}OH + HO_2^{\bullet}$	2.18×10^{10}	−0.72	34813	304,44
39	$O_2 + H_2O_2 \Rightarrow HO_2^{\bullet} + HO_2^{\bullet}$	4.53×10^8	−0.39	19700	175,35
40	${}^{\bullet}OH + {}^{\bullet}OH + M \Rightarrow H_2O_2 + M$; Coef. H_2: 2.5, H_2O: 16.0	9.0×10^{-1}	0.90	−3050	-217,89
41	$H_2O + {}^{\bullet}OH \Rightarrow H_2O_2 + H^{\bullet}$	1.14×10^3	1.36	38180	290,93
42	$H_2 + HO_2^{\bullet} \Rightarrow H_2O_2 + H^{\bullet}$	1.41×10^5	0.66	12320	64,32
43	${}^{\bullet}OH + HO_2^{\bullet} \Rightarrow H_2O_2 + O$	4.62×10^{-3}	2.75	9277	56,08
44	$H_2O + HO_2^{\bullet} \Rightarrow H_2O_2 + {}^{\bullet}OH$	2.8×10^7	0	16500	128,67
45	$O_2 + O + M \Rightarrow O_3 + M$; Coef. O_2: 1.64; Coef. O_2: 1.63, H_2O: 15	4.1	0	−1057	-109,27

Table 3. Electrochemical and chemical scheme of the possible reactions occurring at the electrodes and in the electrolyte by the Sono-Galvano Fenton-based processes. k_i is the absolute reaction constant of the i[th] reaction. Adapted from Bray (1931) and Koprivanac & Lonˇ(2006) and De Laat & Le 2006 and Machulek et al. (2009).

	i	i[th] Reaction	k_i	Unit of k_i
Anode	1	$Fe \rightarrow Fe^{2+} + 2e^-$	-	-
Cathode	2	$2\,H^+ + 2e^- \rightarrow H_2$	-	-
	3	$Fe^{2+} + H_2O_2 \rightarrow Fe^{3+} + OH^- + HO^\bullet$	6.3×10^{-2}	$mol^{-1}.m^3.s^{-1}$
	4	$Fe^{3+} + H_2O_2 \rightarrow Fe(HO_2)^{2+} + H^+$	3.1×10^{4}	$mol^{-1}.m^3.s^{-1}$
	5	$Fe(HO_2)^{2+} + H^+ \rightarrow Fe^{3+} + H_2O_2$	1.0×10^{7}	$mol^{-1}.m^3.s^{-1}$
	6	$Fe(HO_2)^{2+} \rightarrow Fe^{2+} + HO_2^\bullet$	2.3×10^{-3}	s^{-1}
	7	$H_2O_2 + HO^\bullet \rightarrow HO_2^\bullet + H_2O$	3.3×10^{4}	$mol^{-1}.m^3.s^{-1}$
	8	$HO_2^\bullet \rightarrow O_2^{\bullet-} + H^+$	1.58×10^{5}	s^{-1}
	9	$O_2^{\bullet-} + H^+ \rightarrow HO_2^\bullet$	1.0×10^{7}	$mol^{-1}.m^3.s^{-1}$
	10	$Fe^{2+} + HO^\bullet \rightarrow Fe^{3+} + OH^-$	3.2×10^{5}	$mol^{-1}.m^3.s^{-1}$
	11	$HO_2^\bullet + Fe^{2+} + H_2O \rightarrow Fe^{3+} + H_2O_2 + OH^-$	1.2×10^{3}	$mol^{-1}.m^3.s^{-1}$
	12	$HO_2^\bullet + Fe^{3+} \rightarrow Fe^{2+} + H^+ + O_2$	3.6×10^{2}	$mol^{-1}.m^3.s^{-1}$
	13	$O_2^{\bullet-} + Fe^{2+} + 2H_2O \rightarrow Fe^{3+} + H_2O_2 + 2\,OH^-$	1.0×10^{4}	$mol^{-1}.m^3.s^{-1}$
	14	$O_2^{\bullet-} + Fe^{3+} \rightarrow Fe^{2+} + O_2$	5.0×10^{4}	$mol^{-1}.m^3.s^{-1}$
	15	$HO^\bullet + HO^\bullet \rightarrow H_2O_2$	5.2×10^{6}	$mol^{-1}.m^3.s^{-1}$
	16	$HO_2^\bullet + HO_2^\bullet \rightarrow H_2O_2 + O_2$	8.3×10^{2}	$mol^{-1}.m^3.s^{-1}$
	17	$O_2^{\bullet-} + H^+ \rightarrow HO_2^\bullet$	1.0×10^{7}	$mol^{-1}.m^3.s^{-1}$
	18	$HO^\bullet + HO_2^\bullet \rightarrow O_2 + H_2O$	7.1×10^{6}	$mol^{-1}.m^3.s^{-1}$
	19	$HO^\bullet + O_2^{\bullet-} \rightarrow O_2 + OH^-$	1.01×10^{7}	$mol^{-1}.m^3.s^{-1}$
Electrolyte	20	$HO_2^\bullet + O_2^{\bullet-} + H_2O \rightarrow H_2O_2 + O_2 + OH^-$	9.7×10^{4}	$mol^{-1}.m^3.s^{-1}$
	21	$HO_2^\bullet + H_2O_2 \rightarrow O_2 + HO^\bullet + H_2O$	5.0×10^{-4}	$mol^{-1}.m^3.s^{-1}$
	22	$O_2^{\bullet-} + H_2O_2 \rightarrow O_2 + HO^\bullet + OH^-$	1.3×10^{-4}	$mol^{-1}.m^3.s^{-1}$
	23	$Fe^{2+} + SO_4^{2-} \rightarrow FeSO_4$	2.29×10^{8}	$mol^{-1}.m^3.s^{-1}$
	24	$SO_4^{2-} + HO^\bullet \rightarrow SO_4^{\bullet-} + OH^-$	1.4×10^{4}	$mol^{-1}.m^3.s^{-1}$
	25	$HSO_4^- + HO^\bullet \rightarrow SO_4^{\bullet-} + H_2O$	3.5×10^{2}	$mol^{-1}.m^3.s^{-1}$
	26	$SO_4^{\bullet-} + H_2O \rightarrow H^+ + SO_4^{2-} + HO^\bullet$	3.0×10^{5}	s^{-1}
	27	$SO_4^{\bullet-} + OH^- \rightarrow SO_4^{2-} + HO^\bullet$	1.4×10^{4}	$mol^{-1}.m^3.s^{-1}$
	28	$SO_4^{\bullet-} + H_2O_2 \rightarrow SO_4^{2-} + H^+ + HO_2^\bullet$	1.2×10^{4}	$mol^{-1}.m^3.s^{-1}$
	29	$SO_4^{\bullet-} + HO_2^\bullet \rightarrow SO_4^{2-} + H^+ + O_2$	3.5×10^{6}	$mol^{-1}.m^3.s^{-1}$
	30	$SO_4^{\bullet-} + Fe^{2+} \rightarrow Fe^{3+} + SO_4^{2-}$	3.0×10^{5}	$mol^{-1}.m^3.s^{-1}$
	31	$FeSO_4 \rightarrow Fe^{2+} + SO_4^{2-}$	1.0×10^{10}	s^{-1}
	32	$Fe^{3+} + H_2O \rightarrow FeOH^{2+} + H^+$	2.9×10^{7}	s^{-1}
	33	$FeOH^{2+} + H^+ \rightarrow Fe^{3+} + H_2O$	1.0×10^{7}	$mol^{-1}.m^3.s^{-1}$
	34	$FeOH^{2+} + H_2O_2 \rightarrow Fe(OH)HO_2^{+} + H^+$	2.0×10^{3}	$mol^{-1}.m^3.s^{-1}$
	35	$Fe(OH)HO_2^{+} + H^+ \rightarrow FeOH^{2+} + H_2O_2$	1.0×10^{7}	$mol^{-1}.m^3.s^{-1}$
	36	$Fe(OH)HO_2^{+} \rightarrow Fe^{2+} + HO_2^\bullet + OH^-$	2.3×10^{-3}	s^{-1}

Each reaction from the previous Table can be schematized according to Eq.16.

$$\sum_{k=1}^{K} v'_{ki} X_k \rightarrow \sum_{k=1}^{K} v''_{ki} X_k \tag{16}$$

v'_{ki} is the stoichiometric coefficient related to the kth species X_k within the ith chemical reaction. The kinetics rate related to the i[th] reaction is expressed as reported in Eq.17.

$$r_i = k_i \prod_{k=1}^{K} [C_k]^{\vartheta' ki} \tag{171}$$

k_i is the kinetic constant related to the i^{th} reaction occurring in the electrolyte among the 36 reactions reported in Table 3 and is determined at the operating temperature of 25 °C in the present study.

The kinetics of apparition and the disappearance of a species X_k in the electrolyte is governed by Eq.18 for species involved in the electrochemical reactions:

$$\frac{d[X_k]}{dt} = \pm\frac{1}{nV}\frac{i_{corr}}{F} + \sum_{i=1}^{N}(v''_{ki} - v'_{ki})\, k_i \prod_{j=1}^{K}[X_j]^{\vartheta'_{ji}} \quad (18)$$

Eq.19 is applicable to species that are only implicated in the electrolytic reactions (Davis & Davis, 2003).

$$\frac{d[X_k]}{dt} = \sum_{i=1}^{N}(v''_{ki} - v'_{ki})\, k_i \prod_{j=1}^{K}[X_j]^{\vartheta'_{ji}} \quad (19)$$

Eq.18 is particularly expressed for hydrogen peroxide as follows, considering the kinetics of production through sonochemistry:

$$\frac{d[H_2O_2]}{dt} = k_0 + \sum_{i=1}^{N}(v''_{ki} - v'_{ki})\, k_i \prod_{j=1}^{K}[X_j]^{\vartheta'_{ji}} \quad (20)$$

The system of non-linear differential equations related to sonochemistry, on one hand, and Sono-Galvano-Fenton, on the other hand, is resolved using the fourth-order Runge–Kutta algorithm on Matlab with a fixed step of 1 s. The simulation is performed over 1200 s.

Results and Discussion

Hydrogen Peroxide Production at Single Bubble Scale

The performed simulations of the sonochemical process under oxygen atmosphere considering the configuration described earlier result in the molar yields of hydrogen peroxide produced at the single bubble scale as shown in Fig.2. The figure demonstrates that the lower the frequency, the higher the yield of sonochemical hydrogen peroxide. This is in good agreement with the fact that harsher conditions of temperature and pressure are retrieved when lower acoustic frequencies are used in sonication within the ultrasonic range. Higher temperature and pressure are probably responsible of the activation of the sonochemical mechanism inside the bubble. Nonetheless, the sonochemical production at the reactor scale should consider the number density of bubbles, which is a parameter that is highly influenced by the acoustic frequency. This will be verified in the following figure.

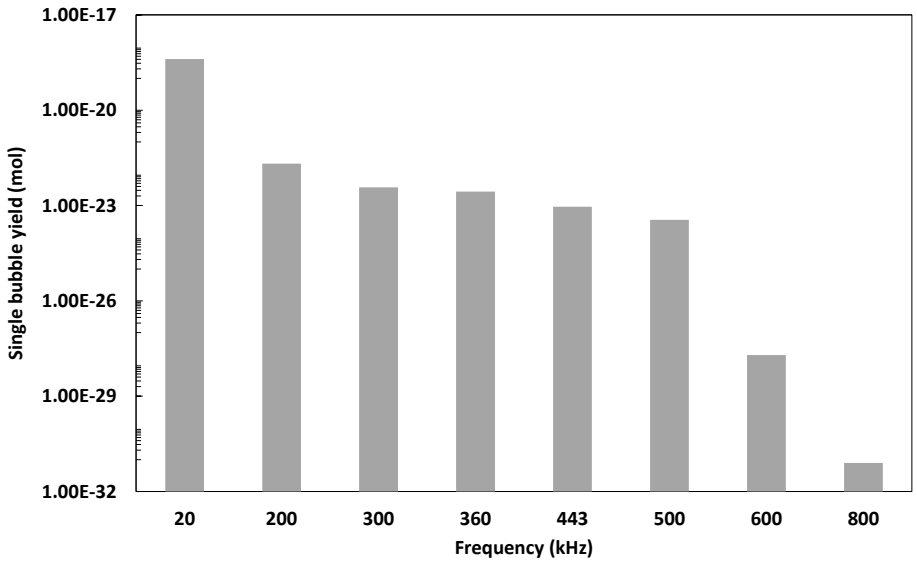

Figure 2. Evolution of H_2O_2 molar yield at single bubble scale as a function of the acoustic frequency under oxygen atmosphere, 1.5 atm of amplitude and within 50 µs od sonication.

Hydrogen Peroxide Production at Reactor Scale

Fig. 3 shows the molar yields of hydrogen peroxide produced sonochemically within a reactional volume of 1 dm^3. The introduction of the number density of bubbles according to Eq.13 completely changes the trend shown previously in Fig. 3. The production at the reactor scale demonstrates a quite stable value for frequencies comprised between 200 and 500 kHz, with a maximum achieved at 200 kHz, of 1.59×10^{-15} mol/dm^3 attained in 50 µs. This leads to a production rate of 0.0318 $\mu mol/s.m^3$ in the electrolyte. This value will be used in the zero-order kinetics adopted for the macroscopic sonochemical production of hydrogen peroxide. It is worthy to mention that 200 kHz has been selected as the optimal frequency for sonication not only as it leads to maximum production of hydrogen peroxide, but also to take benefit of the relatively low frequency role in physical effects, contributing to mixing and transport phenomena.

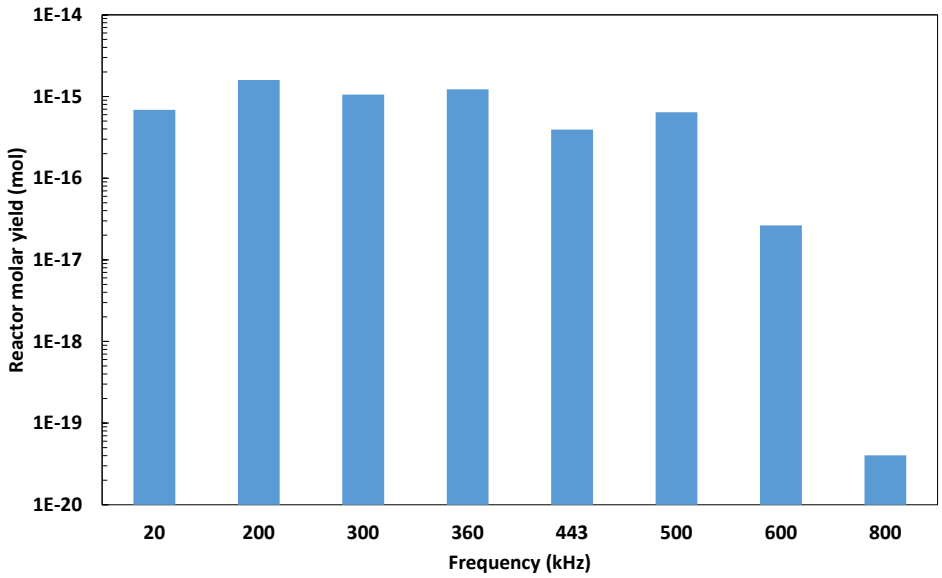

Figure 3. Evolution of H_2O_2 molar yield at reactor scale of a volume of 1 dm^3 as a function of the acoustic frequency under oxygen atmosphere, 1.5 atm of amplitude and within 50 µs of sonication.

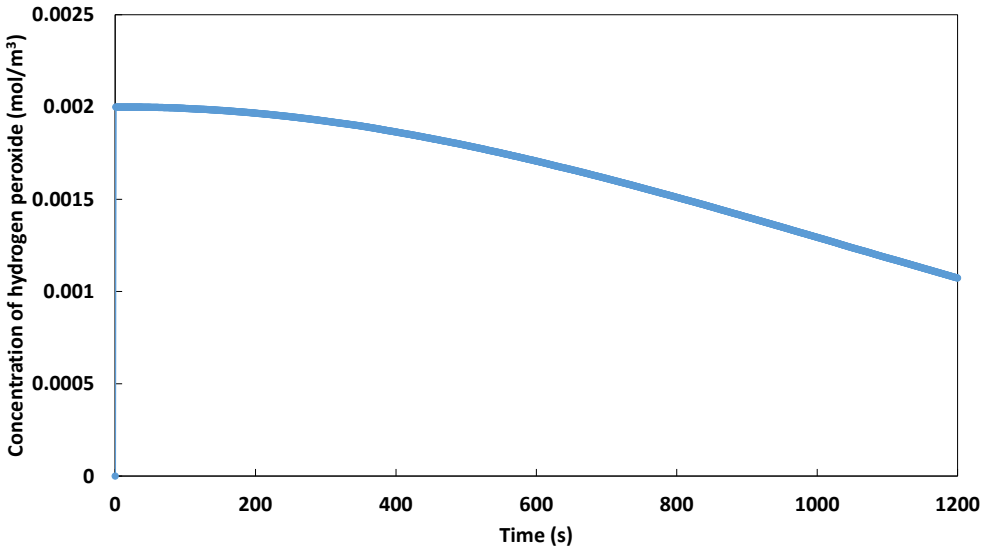

Figure 4. Evolution of the concentration of hydrogen peroxide in the electrolyte

Integrated Sono-Galvano-Fenton Process

The kinetics of hydrogen peroxide in the integrated process is investigated considering the sonochemical production rate mentioned in the previous paragraph. Fig.4 reports the evolution of the concentration of

hydrogen peroxide taking into account all the reactions that involve it, i.e., the sonochemical reactions mentioned in Table.2 and the electrolytic reactions mentioned in Table.3. Within 1200 s of operation, the concentration of hydrogen peroxide passes from 0.002 mol/m^3 to 0.0011 mol/m^3, with a negative exponential trend.

Hydrogen peroxide is implicated in the main Fenton reaction, where it decomposes to hydroxyl radials in the presence of ferrous ions provided by the Galvano-Fenton process. The evolution of the concentration of hydroxyl radical coming from the integrated Sono-Galvano-Fenton process is reported in Fig.5, the evolution of the concentration of the same radical induced by the sonochemical process is also reported in the same figure.

Surprisingly, the sonochemical process is able to provide 10^5 folds higher yield of hydroxyl radical, while producing the Fenton reagent to the Sono-Galvano-Fenton process. This makes evidence for an upscaled configuration of the Sono-Galvano-Fenton process based on the multiplication of the number of galvanic cells to put in the process (scaling out), while maintaining the configuration of the sonochemical process integrated to the parallel galvanic cells.

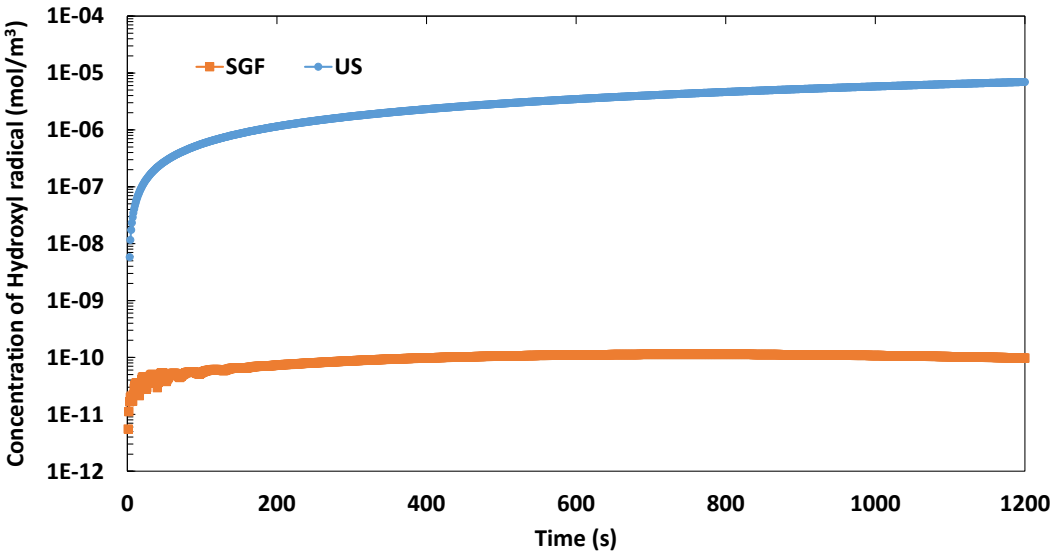

Figure 5. Evolution of the concentration of hydroxyl radical within the integrated Sono-Galvano-Fenton reactor

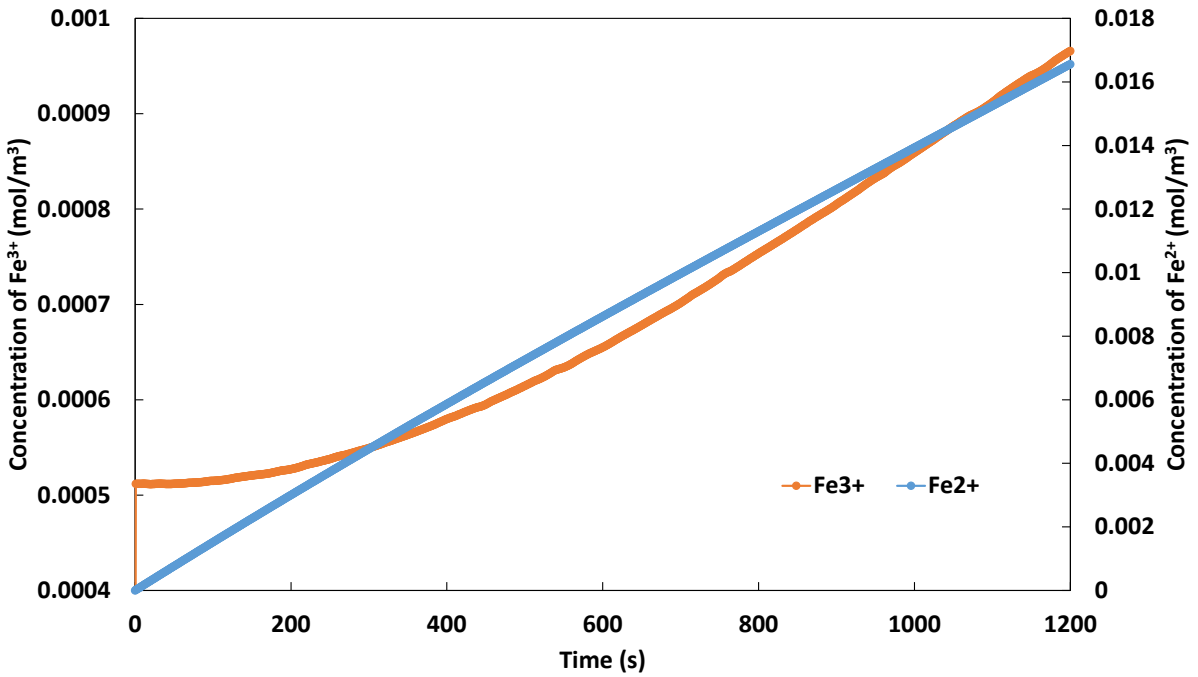

Figure 6. Evolution of the concentration of ferric and ferrous ions during the Sono-Galvano-Fenton operation

We suggest in the following to evaluate the kinetics of ferrous and ferric ions in the electrolyte during the operation of the Sono-Galvano-Fenton process. Fig.6 shows the evolution of the concentrations of both ions as function of time. We notice that the evolution of ferrous ions is quasi-linear, starting from zero at the initial time, since no catalyst is added to the electrolyte.

The linear trend is well justified by the Faraday's law, governing the spontaneous corrosion of iron waste under the potential induced by the copper cathode. Simultaneously, ferric ions produced by the reaction of hydrogen peroxide and ferrous ions, but also responsible of the regeneration of ferrous ions (the catalyst) through reactions 4, 5 and 6 reported in Table. 3, show a quite different curve of evolution in function of time. Ferric ions are produced rapidly at the initial time, then evolve exponentially due to the simultaneous production and consumption in the regeneration reaction, with the upper hand to the production reaction. The regeneration reactions are indeed known to be slow (I. Gasmi et al. 2020; Intissar Gasmi et al. 2021), and consequently, the source of ferrous ions should provide continuously sufficient yield of catalyst to maintain a high reactional rate of Fenton mechanism.

Secondary Physical Effects of Ultrasounds

In this last section, we propose to investigate the secondary role of ultrasounds in the integrated process, namely the possible physical effects inducing the enhancement of the mixing and transport phenomena in the electrolyte, particularly through shockwaves and microjets. The microscopic powers associated to the microjet and shockwave emitted by the bubble around the collapse have been assessed and their evolution during this time slot is reported in Fig.7.

The figure shows that the time intervals preceding and following immediately the instant of harsh collapse are characterized by a high power related to microjet, while the instant of harsh collapse exhibits a maximum power related to shockwave, both of them are in the order of magnitude of 1 W. Hence, the sonication at 200 kHz has obviously a chemical role demonstrated through the production of hydroxyl radicals and hydrogen peroxide as a feedstock for Fenton reaction, but may also play a physical role by improving the transport phenomena and mixing of the electrolyte and consequently enhancing the corrosion current. This track will be the subject of upcoming studies of our research group.

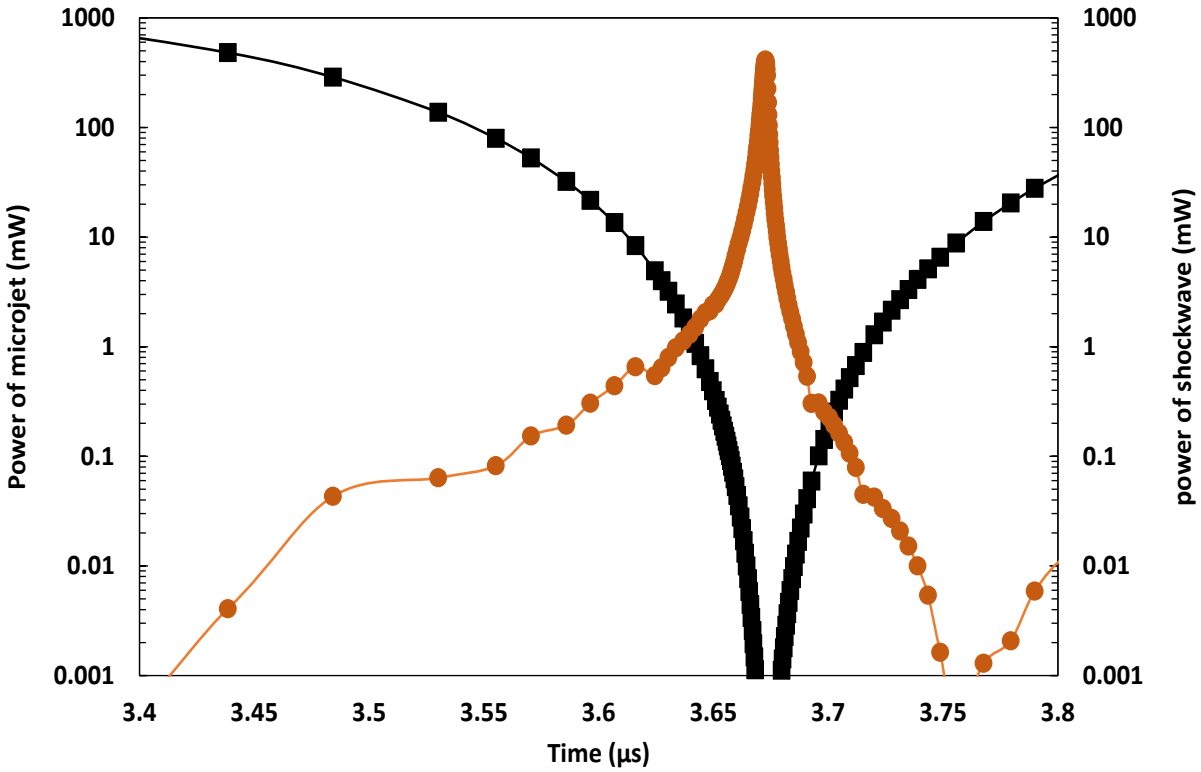

Figure 7. Powers associated with the secondary physical effects of the acoustic cavitation bubble around its collapse (microjet in black and shockwave in orange)

Conclusion

The investigation of the isolated sonochemical effect at single bubble scale demonstrated that the lower the frequency, the higher the yield of sonochemical hydrogen peroxide. However, at the reactor scale, 200 kHz has been selected as the optimal frequency for sonication not only as it leads to maximum production of hydrogen peroxide, but also to take benefit of the relatively low frequency role in physical effects, contributing to mixing and transport phenomena.

In the integrated Sono-Galvano-Fenton process, within 1200 s of operation, the concentration of hydrogen peroxide passes from 0.002 mol/m^3 to 0.0011 mol/m^3, with a negative exponential trend. The investigation of the production of hydroxyl radicals in the integrated process has shown that the sonochemical process is able to provide 10^5 folds higher yield of hydroxyl radical, while producing the Fenton reagent to the Sono-Galvano-Fenton process. This makes evidence for an upscaled configuration of the Sono-Galvano-Fenton process based on the multiplication of the number of galvanic cells to put in the process (scaling out), while maintaining the configuration of the sonochemical process integrated to the parallel galvanic cells. In terms of ferrous and ferric ions kinetics in the integrated process, the regeneration reactions proved to be slow as demonstrated in several previous studies, and consequently, the source of ferrous ions should provide continuously sufficient yield of catalyst to maintain a high reactional rate of Fenton mechanism.

In terms of the physical effects of mechanical nature, the study at the single bubble scale proved that microjet achieve the highest power values around the collapse instant, while shockwave does at the instant of the harsh collapse with a value of 1 W. The sonication at 200 kHz has obviously a chemical role demonstrated through the production of hydroxyl radicals and hydrogen peroxide as a feedstock for Fenton reaction, but may also play a physical role by improving the transport phenomena and mixing of the electrolyte and consequently enhancing the corrosion current. This track will be the subject of upcoming studies of our research group.

Scientific Ethics Declaration

The author declares that the scientific ethical and legal responsibility of this article published in EPSTEM journal belongs to the author.

Acknowledgements or Notes

* This article was presented as an oral presentation at the International Conference on Technology (www.icontechno.net) held in Antalya/Turkey on November 16-19, 2023.

*This work was financially supported by the National Direction for Research and Technological Development DGRSDT, Algeria, in the frame of the “PISE” project entitled “GreEnAREA”, supported by the mixed team of research “PVA” and affiliated to the National Higher School of Technology and Engineering.

References

Ahmad, Z.(.2006). Corrosion kinetics. In B. T. Zaki (Ed.), *Principles of Corrosion Engineering and Corrosion Control Ahmad* (pp.57-119). Oxford: Butterworth-Heinemann.

Atchley, A. A. (1989). The blake threshold of a cavitation nucleus having a radius-dependent surface tension.” *The Journal of the Acoustical Society of America*, *85*(1), 152–57.

Authier, O., Ouhabaz, H., & Bedogni, S.(2018). Modeling of sonochemistry in water in the presence of dissolved carbon dioxide.*Ultrasonics Sonochemistry*, *45*,17–28.

Barbusinski, K. (2009). Fenton reaction - controversy concerning the chemistry. *Ecological Chemistry and Engineerings*, *16*(3), 347–358.

Baulch, D. L., Drysdale, D. D. D., Duxbury, J., & Grant,S. (1972). *Evaluated kinetic data for high temperature reactions* (Vol. 1): *Homogeneous gas phase reactions of the O2—O3 systems, the CO—O2— H2 system, and of sulphur-containing species* .

Baulch, D. L., Drysdale, D. D. D., Duxbury, J., & Grant,S. (1974). *Evaluated kinetic data for high temperature reactions* (Vol. 2): *Homogeneous gas phase reactions of the O2—O3 systems, the CO—O2— H2 system, and of sulphur-containing species* .

Baulch, D. L., Drysdale, D. D. D., Duxbury, J., & Grant,S. (1976). *Evaluated kinetic data for high temperature reactions* (Vol. 3): *Homogeneous gas phase reactions of the O2—O3 systems, the CO—O2— H2 system, and of sulphur-containing species* .

Bray, W.C. (1931). The mechanism of reactions in aqueous solution examples involving equilibria and steady states. *Chemical Reviews*, *10*(1), 161–177.

Brotchie, A., Grieser, F., & Ashokkumar, M. (2009). Effect of power and frequency on bubble-size distributions in acoustic cavitation. *Physical Review Letters*, *102*(8), 1–4.

Dalodiere, E., Matthieu, V., Philippe, M., & Sergey I. N. (2016). Effect of ultrasonic grequency on H2O2 sonochemical formation rate in aqueous nitric acid Solutions in the Presence of Oxygen." *Ultrasonics Sonochemistry*, *29*(2), 198–204.

Davis, M. E., & Robert, J., & Davis, R. J. (2003). *The basics of reaction kinetics for chemical reaction engineering fundamentals of chemical reaction engineering* (pp.1-52). New York, NY: McGraw Hill. Retrieved from http://resolver.caltech.edu.

De Laat, J., & Le, T.G. (2006). Effects of chloride ions on the iron(III)-catalyzed decomposition of hydrogen peroxide and on the efficiency of the fenton-like oxidation process. *Applied Catalysis B: Environmental*, *66*(1–2), 137–146.

Gasmi, I., Kerboua, K., Haddour, N., & Hamdoui,O. (2020). Kinetic pathways of iron electrode transformations in galvano-fnton process: A mechanistic investigation of in-situ catalyst formation and regeneration. *Journal of the Taiwan Institute of Chemical Engineers*, *116*(2020), 1–11.

Gasmi, I., Kerboua, K., Haddour, N., Hamdoui,O., Alghyamah, A., & Buret, F. (2021).The Galvano-Fenton process: Experimental insights and numerical mechanistic investigation applied to the degradation of acid orange 7. *Electrochimica Acta*, *373*.

He, Y. Z., Mallard, W. G., & Tsang, W. (1988). Kinetics of hydrogen and hydroxyl hadical attack. *Journal of Physical Chemistry*, *92*(8), 2196–2201.

Kamath, V., Prosperetti, A., & Egolfopoulos, F. N. (1993). A theoretical study of sonoluminescence. *Journal of the Acoustical Society of America*, *94*(1), 248–260.

Kerboua, K.(2022). Water remediation from recalcitrant pollution using the Galvano-Fenton process : A modeling approach of the hydroxyl radical generation and the energy efficiency.*The Eurasia Proceedings of Science, Technology, Engineering & Mathematics*, *21*, 506–516.

Kerboua, K., & Hamdaoui, O. (2017). Computational study of state equation effect on single acoustic cavitation bubble's phenomenon. *Ultrasonics Sonochemistry*, *38*, 174–188.

Kerboua, K., & Hamdaoui, O. (2018).Ultrasonic waveform upshot on mass variation within single cavitation bubble: Investigation of physical and chemical transformations.*Ultrasonics Sonochemistry*, *42*, 508–516.

Kerboua, K., & Hamdaoui, O. (2019). Void fraction , number density of acoustic cavitation bubbles and acoustic frequency : A numerical investigation. *The Journal of the Acoustical Society of America*, *146*(4), 2240–2252.

Kerboua, K., Hamdaoui, O., Haddour, N., & Alghyamah, A.(2021). Simultaneous Galvanic generation of Fe2+ catalyst and spontaneous energy release in the Galvano-Fenton technique : A numerical investigation of Phenol's oxidation and energy production and saving. *Catalysts*, *11*(943).

Koprivanac, N., & Lon, A. (2006). Photo-assisted fenton type processes for the degradation of phenol : A kinetic study. *Journal of Hazardous Materials*, *136*, 632–644.

Langlois, T. R., Changxi, Z., & Doug L. J. (2016). Toward animating water with complex acoustic bubbles.*ACM Transactions on Graphics*, *35*(4), 1–13.

Leighton, T. G. (1994). The acoustic bubble. *The Journal of the Acoustical Society of America*, *96*(4).

Machulek, A., de Moraes, J. E. F., Okano, L.T., & Silverio, C. A. (2009). Photolysis of ferric ions in the presence of sulfate or chloride ions : Implications for the photo-fenton process. *Photochemical & Photobiological Sciences*, *8*(7), 985–991.

Mason, T. J. (1999). Sonochemistry : Current uses and future prospects in the chemical. *Phiosophical Transactions of the Royal Society*, *357*(1751), 355–369.

Mason, T. J. (1999). Sonochemistry : Current uses and future prospects in the chemical. *Phiosophical Transactions of the Royal Society*, *357*(1751), 355–369.

Minnaert, M. (1933). XVI on musical air-bubbles and the sounds of running water . *The London, Edinburgh, and Dublin Philosophical Magazine and Journal of Science*, *16*(104), 235–248.

Palit, S. (2012). An overview of advanced oxidation process as an effective and visionary environmental engineering procedure to treat dye effluents from textile industries. *IEEE International Conference on Engineering Education: AICERA*, 1–1.

Yasui, K. (1996). Variation of liquid temperature at bubble wall near the sonoluminescence threshold. *Journal of the Physical Society of Japan*, *65*(9), 2830–40.

Yasui, K.(1997). Alternative model of single bubble sonoluminescence. *Physical review E*, *56*(6), 6750–6760.

Yasui,K. (2002). Influence of ultrasonic frequency on multibubble sonoluminescence. *The Journal of the Acoustical Society of America*, *112*(4), 1405– 1413.

Ziembowicz, S., Małgorzata, K., & Koszelnik, P. (2017). Sonochemical formation of hydrogen peroxide. *Proceedings*, *2*(5), 188.

Author Information

Kaouther Kerboua
Department of Process and Energy Engineering,
National Higher School of Technology and Engineering,
23005, Annaba, Algeria
Contact e-mail: *k.kerboua@ensti-annaba.dz*

To cite this article:

Kerboua, K. (2023). A numerical study of the efficiency of the sono Galvano Fenton process as a tertiary treatment technique for the wastewater reuse in agriculture. *The Eurasia Proceedings of Science, Technology, Engineering & Mathematics (EPSTEM), 24*, 243-256.